

Article

# A Self-Adaptive Damping Control Strategy of Virtual Synchronous Generator to Improve Frequency Stability

Tianyang Li <sup>1,2</sup>, Buyang Wen <sup>1,2,\*</sup> and Huaiyuan Wang <sup>1,2</sup>

<sup>1</sup> Fujian Smart Electrical Engineering Technology Research Center, College of Electrical Engineering and Automation, Fuzhou University, Fuzhou 350116, China; n180127036@fzu.edu.cn (T.L.); wenby87@fzu.edu.cn (B.W.); wanghuaiy@stu.xjtu.edu.cn (H.W.)

<sup>2</sup> Jinjiang Science and Education Park of Fuzhou University, Fuzhou University, Quanzhou 362200, China; n180127036@fzu.edu.cn

\* Correspondence: wenby87@fzu.edu.cn

Received: 10 February 2020; Accepted: 2 March 2020; Published: 4 March 2020

**Abstract:** In a microgrid, grid-connected inverters, as the interface between the distributed power supply and grid, cannot provide inertia support for the system. The control strategy of virtual synchronous generator (VSG) based on grid-connected inverters can enhance the stability of system frequency. In order to make the frequency response that has a smaller overshoot and a shorter settling time, a self-adaptive damping control strategy based on the relationship between the damping and the maximum frequency deviation for microgrid VSG is presented. The small-signal mathematical model of VSG is established, and the range of the damping coefficient is determined. Finally, simulation experiments are carried out with MATLAB/Simulink, and the effectiveness of the proposed control strategy is verified by comparing it with various damping control methods.

**Keywords:** virtual synchronous generator; frequency stability; self-adaptive control; damping

## 1. Introduction

Influenced by the global energy crisis, the penetration rate of the distributed power generation system using renewable energy is increasing. As the interface between most distributed energy and power grid, grid-connected inverters play an important role in transmitting power to the power grid [1–3]. Unlike the synchronous generator (SG), the inverters based on power electronics technology have almost no internal inertia, which affects the stability of the power system and cannot provide frequency and voltage support for the power grid with distributed generation.

In order to make new energy that has a certain frequency support capability, the droop control strategy is usually adopted in the inverter [4–7]. The droop control is to simulate the droop characteristics of SGs. When the frequency and voltage of the systems change, the output active power and reactive power of inverters change according to the droop characteristic. However, the droop control only simulates the primary frequency regulation and the primary voltage regulation characteristics of the SG. The inertial support capability of the SG is not realized.

In the power system, because the rotor of the SG has inertia, the frequency fluctuation can be restrained and the stability of power grid operation is enhanced. According to this idea, the concept of virtual synchronous generator (VSG) is proposed in References [8–13]. By introducing the mechanical and electromagnetic equations of the SG, its mechanism and external characteristics are simulated by the inverter.

However, the addition of virtual inertia may aggravate the oscillation of active power after a disturbance. Therefore, the proper damping effect needs to be introduced into VSG [10,11]. In

Reference [12], the damping algorithm proposed by linear control theory can effectively avoid the low-frequency oscillation after disturbance. In Reference [14], various kinds of damping effect in VSG are compared. A generalized droop control strategy is proposed. According to the dynamic response requirements of VSG frequency and output power, the zero and pole positions of the closed-loop transfer function are set. In Reference [15], the damping power includes the frequency deviation, the output power, and the integral of the damping power multiplied by their respective proportional coefficients. According to the desired closed-loop eigenvalue of the system, the coefficients are obtained by the state feedback method. In Reference [16], a differential term for the output power is added to the active power loop, and the damping ratio of the system can be freely adjusted without affecting the steady-state frequency droop characteristics.

In addition to the above fixed-parameter strategies, some adaptive parameter methods are also proposed. In Reference [17], the relationship between the damping coefficient and frequency stability is summarized. Then, an adaptive damping algorithm based on frequency deviation is presented. However, the damping coefficient only increases when the frequency tends to be steady. The effect of the damping coefficient is not fully exerted. In Reference [18], the damping coefficient increases exponentially based on the frequency deviation, so that the overshoot of the output power can be reduced, but the damping coefficient increases only when the frequency deviation is large. The damping coefficients in the most existing literature is set according to the preset maximum frequency deviation. However, in the actual process, the frequency may not reach the preset maximum deviation value. The control capability of the inverter is not fully utilized.

In this paper, the influence of damping on the dynamic characteristics and steady-state performance of VSG system is analyzed. The maximum deviation of the frequency is dynamically measured. The damping coefficient is adjusted based on the maximum frequency deviation. The dynamic characteristics of the frequency response are improved. Through VSG active power loop and small-signal mathematical model, the range of the damping coefficient is determined. Finally, the damping algorithm in this paper is compared with the fixed damping method and the damping method based on the frequency deviation. The effectiveness of the proposed algorithm is verified by the simulation experiment with MATLAB/Simulink.

## 2. Basic Principles of VSG

Figure 1 is the main circuit topology and control block diagram of grid-connected inverters. It mainly includes distributed power, energy storage system, three-phase inverter bridge, LCL filter, and local load. The LCL filter is composed of the inverter-side inductor  $L_1$ , the filter capacitor  $C$ , and the grid-side inductor  $L_2$ . The output voltage  $u_a, u_b, u_c$  and current  $i_a, i_b, i_c$  of the LCL filter are calculated to get the output active power  $P_e$  and the output reactive power  $Q_e$ . The reference voltage  $E_r$  and power angle  $\theta$  are calculated by substituting the set active power  $P_m$  and reactive power  $Q_{set}$  into the VSG control module. Three-phase modulation waves  $e_{ma}, e_{mb}, e_{mc}$  are obtained through voltage and current closed-loop control. Three-phase modulation waves drive each switch of three-phase inverters through pulse width modulation (PWM).

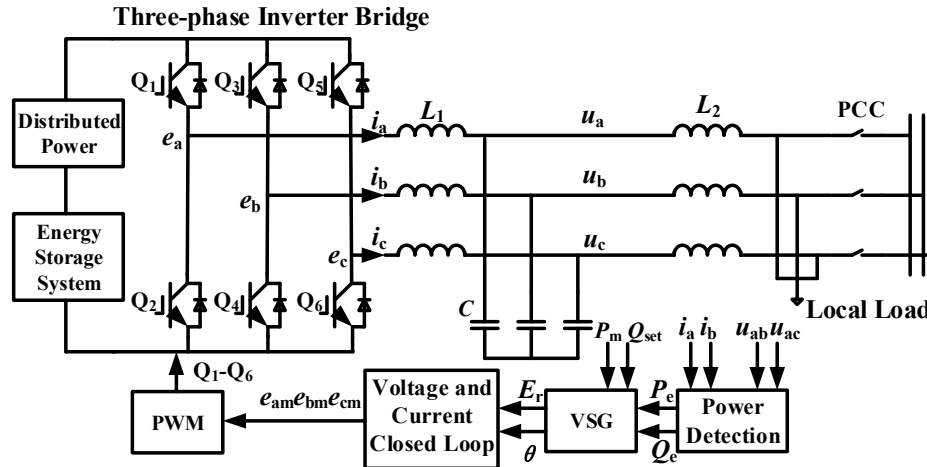


Figure 1. Principle block diagram of virtual synchronous generator (VSG).

The rotor motion equation of the SG is simulated by the active power loop, which makes the distributed generation have the basic characteristics of the SG. In addition, no excessive transient process is introduced. Therefore, the second-order model of the SG is adopted, as shown in Equation (1).

$$\begin{cases} J \frac{d\omega}{dt} = \frac{P_m}{\omega_0} - \frac{P_e}{\omega_0} - D_p (\omega - \omega_g) \\ \frac{d\theta}{dt} = \omega \end{cases} \quad (1)$$

Here,  $J$  is the virtual inertia, which represents the inertia effect of SGs, here is a parameter of the inverter.  $P_m$  is the set value of active power.  $P_e$  is the output active power. When the number of pole pairs  $p = 1$ , the mechanical angular velocity  $\omega$  of the SG is the electrical angular frequency.  $\omega_0$  is the rated angular frequency.  $\omega_g$  is the grid angular frequency.  $D_p$  is the damping coefficient of the inverter, which represents the function of the damper winding.  $\theta$  is the power angle of the SG.

In Equation (1), the damping power is realized by simulating the effect of the damping winding. This requires the addition of a phase-lock loop (PLL) to detect the grid frequency. However, the addition of PLL will delay the dynamic response of VSG and even affect the stability of the system [15]. Therefore, the rated frequency  $\omega_0$  is usually used to replace the grid frequency  $\omega_g$  to generate damping power  $P_D$ , as shown in Equation (2).

$$P_D = D_p (\omega - \omega_0) \quad (2)$$

In the island mode, the integrator  $k_i/s$  is added to the active power loop.  $k_i$  is the integral term coefficient. The PI regulator in the active power loop is composed of the integral term and the damping factor  $D_p$ , to realize the undifferentiated tracking of the rated frequency. The active power loop control block diagram is shown in Figure 2.



frequency enters and maintains in the steady-state interval) of oscillation are two key indicators to judge the frequency stability of the system. The closed-loop transfer function of the frequency loop in VSG is a second-order system. When the value of  $D_p$  is in the under-damped range, according to the automatic control principle [19], the overshoot and the settling time of frequency response decrease with the increase of  $D_p$ . Thus, the stability of system frequency can be enhanced by increasing  $D_p$  in a certain range.

The standard EN 50438 [20] specifies that the continuous operation condition of the inverters connected to the power grid. The frequency of the power grid is maintained between 49 Hz and 51 Hz. Meanwhile, in order to suppress the oscillation of active power and frequency of VSG in the dynamic process, the damping coefficient should be proportional to the rated capacity of the inverter. According to the above criteria, the initial damping coefficient setting principle is obtained. The rated capacity of a single inverter is assumed to be 10 kV·A. When the power grid frequency deviation  $\Delta f_N$  is equal to 1 Hz, the output active power of the inverters changes 100% ( $\Delta P_{\max} = 10$  kW).

In Equation (4),  $\Delta T_{\max}$  is the maximum torque variation,  $\Delta P_{\max}$  is the maximum change of active power, and  $\Delta \omega_{\max}$  is the maximum frequency variation.

$$D_p = \frac{\Delta T_{\max}}{\Delta \omega_{\max}} = \frac{\Delta P_{\max}}{\omega_0 \Delta \omega_{\max}} = \frac{\Delta P_{\max}}{2\pi \omega_0 \Delta f_N} = 5 \text{ Nm} \cdot \text{s} / \text{rad} \quad (4)$$

The fluctuation range of the frequency after disturbance cannot be predicted, so  $\Delta f_N$  is used as the maximum value of frequency variation to set  $D_p$ . As shown in Figure 3, the active load suddenly increases at a certain time, and the frequency drops to the minimum value  $f_{\min}$ . At this time, the deviation between the frequency and the steady-state value is  $\Delta f_1$ . This frequency is less than the maximum allowable variation of the frequency  $\Delta f_N$ . After the frequency reaches the minimum value for the first time,  $\Delta f_1$  can be used instead of  $\Delta f_N$  to set a new damping coefficient  $D_{p1}$  as shown in Equation (5). The relationship between the maximum frequency deviation and the damping is dynamically considered. This damping coefficient is about 5 times that of the initial value so that the frequency response has a shorter settling time and a smaller overshoot.

$$D_{p1} = \frac{\Delta P_{\max}}{\omega_0 \Delta \omega_{\max 1}} = \frac{\Delta P_{\max}}{2\pi \omega_0 \Delta f_1} \quad (5)$$

When the frequency rises from the minimum  $f_{\min}$  to the maximum  $f_{\max}$ , the difference between the maximum  $f_{\max}$  and the steady-state value is  $\Delta f_2$ . At this time,  $\Delta f_2$  can be used instead of  $\Delta f_1$  to set a larger damping coefficient. The oscillation of the frequency is greatly slowed down, and the frequency is returned to the steady-state interval more quickly. In Figure 3, the initial damping of three curves is the same. The damping coefficient of the curve I is a fixed initial value. The damping of the curve II is set to  $D_{p1}$  at  $f_{\min}$  and kept at that value. The damping coefficient of the curve III is changed to  $D_{p2}$  at  $f_{\max}$  and the value is maintained until the end.

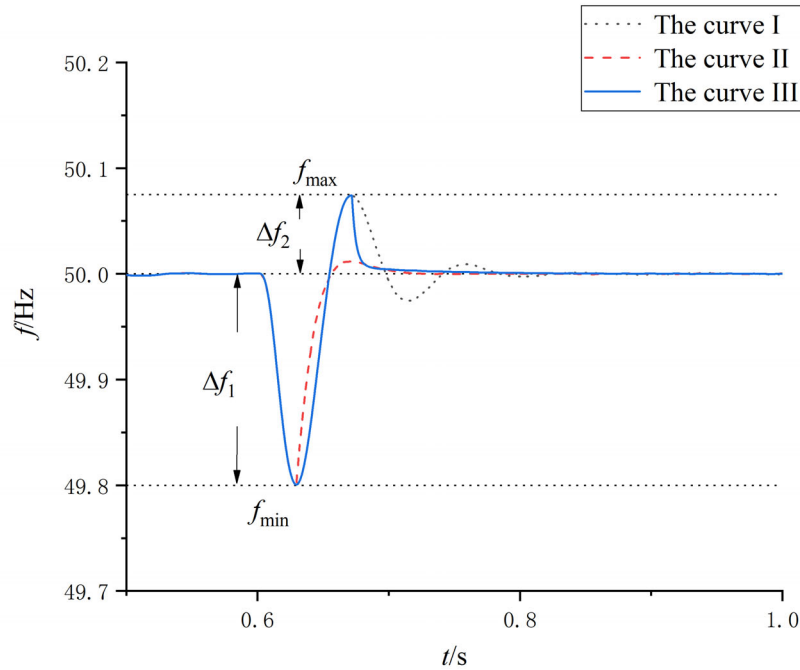


**Figure 3.** Frequency change trend of active load shedding.

The setting process of the damping coefficient is as follows:

1. If the frequency is disturbed and the absolute value is greater than 0.02 Hz, the evaluation is started.
2. When the frequency reaches the extreme value each time, use the frequency deviation  $\Delta f$  at this time to set a new damping coefficient.
3. Compare the setting damping with the preset maximum value. If it is greater than the maximum value, set it according to the maximum value.
4. When the frequency is kept in a stable interval for 2 s, the damping coefficient returns to the initial value.

The setting method of the maximum value will be given in the next chapter.

## 4. Frequency Stability Analysis

### 4.1. The Small-Signal Model

The equivalent circuit in the island mode of the inverter power supply is shown in Figure 4. The output voltage of the inverter is  $E \angle \delta$ ,  $R_1 + jX_1$  is the line impedance,  $Z_L$  is the load impedance, and the output apparent power of the inverter is  $S = P + jQ$ . The sum of the line impedance and load impedance is assumed to be  $R + jX$ . The output apparent power from the inverter power supply is shown in Equation (6). Note that in some cases, when the line impedance is unknown, an online measurement system or an intelligent control structure such as References [21,22] can be applied.

$$S = \frac{U^2}{Z} = \frac{RE^2 \cos 2\varphi + XE^2 \sin 2\varphi}{R^2 + X^2} + j \frac{RE^2 \sin 2\varphi - XE^2 \cos 2\varphi}{R^2 + X^2} \quad (6)$$

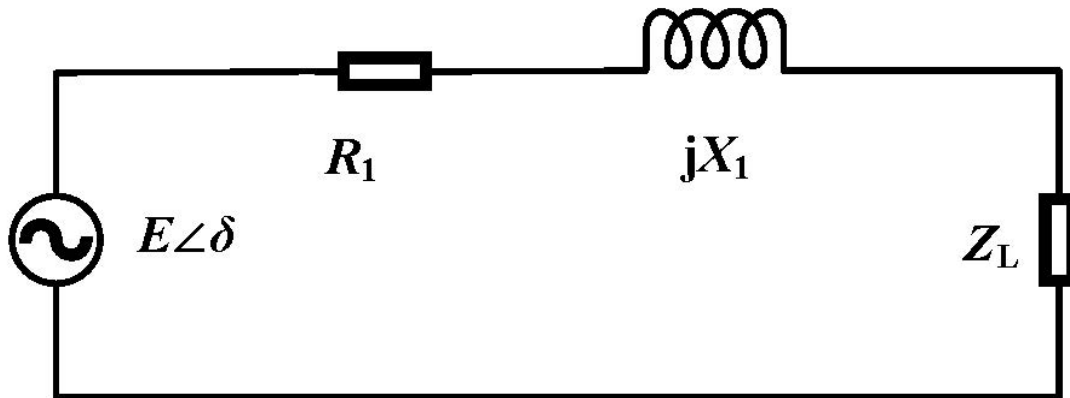


Figure 4. Equivalent circuit of the inverter under island mode.

The static working point is set to  $(E_s, \delta_s)$ . The influence of voltage disturbance  $\Delta E$  and power angle disturbance  $\Delta \delta$  on the output power are considered. The active power and reactive power of the inverter in the autonomous mode are as shown in Equation (7):

$$\begin{cases} \Delta P = \frac{\partial P}{\partial \delta} \Delta \delta + \frac{\partial P}{\partial E} \Delta E = K_{pf} \Delta \delta + K_{pe} \Delta E \\ \Delta Q = \frac{\partial Q}{\partial \delta} \Delta \delta + \frac{\partial Q}{\partial E} \Delta E = K_{qf} \Delta \delta + K_{qe} \Delta E \end{cases} \quad (7)$$

$$\begin{aligned} K_{pf} &= \frac{2XE_s^2 \cos 2\delta_s - 2RE_s^2 \sin 2\delta_s}{R^2 + X^2} \\ K_{pe} &= \frac{2RE_s \cos 2\delta_s + 2XE_s \sin 2\delta_s}{R^2 + X^2} \\ K_{qf} &= \frac{2RE_s^2 \cos 2\delta_s + 2XE_s^2 \sin 2\delta_s}{R^2 + X^2} \\ K_{qe} &= \frac{2RE_s \sin 2\delta_s - 2XE_s \cos 2\delta_s}{R^2 + X^2} \end{aligned} \quad (8)$$

In order to simplify the analysis, the active power and reactive power loops are regarded as approximate decoupling. In combination with Equation (7), the perturbation separation and the

linearization of the time domain equation are carried out. Then, the Laplace change of the linearized time domain equation is carried out. The small-signal model of VSG in the s domain is obtained.

According to the parameter design method in literature [23], the parameters of VSG control system are given in Table 1.

**Table 1.** VSG control system parameters.

Parameters	Values	Parameter	Values
$U_{dc}$	800 V	$C$	10 $\mu$ F
$U_{rms}$	220 V	$L_2$	800 $\mu$ H
$P_N$	10 kW	$E_s$	226 V
$f_N$	50 Hz	$\delta_s$	0.05
$L_1$	3.2 mH	$K_{pwm}$	400
$k_i$	780		

#### 4.2. Damping Parameter Settings

When the microgrid runs off-grid, the output frequency of the inverters is no longer supported by the grid but adjusted by the droop control with inertia. Therefore, the control objective of the off-grid state is to make the output frequency have good dynamic characteristics and steady-state performance. According to the control block diagram of the active power loop in Figure 5, the closed-loop transfer function of the active power-frequency loop is obtained, as shown in Equation (9).

$$G_{p-\omega}(s) = \frac{\omega - \omega_0}{P_m - P_e} = \frac{s}{J\omega_0 s^2 + D_p \omega_0 s + k_i \omega_0} \quad (9)$$

This closed-loop transfer function is a typical second-order system. The natural oscillation angular frequency and the damping ratio are, respectively:

$$\begin{cases} \omega_n = \sqrt{\frac{k_i}{J}} \\ \zeta = \frac{D_p}{2\sqrt{Jk_i}} \end{cases} \quad (10)$$

It can be seen from Equation (10) that the damping ratio of this second-order model is independent of the line impedance. When the line parameters are unknown, the tuning of the damping coefficient is not affected.

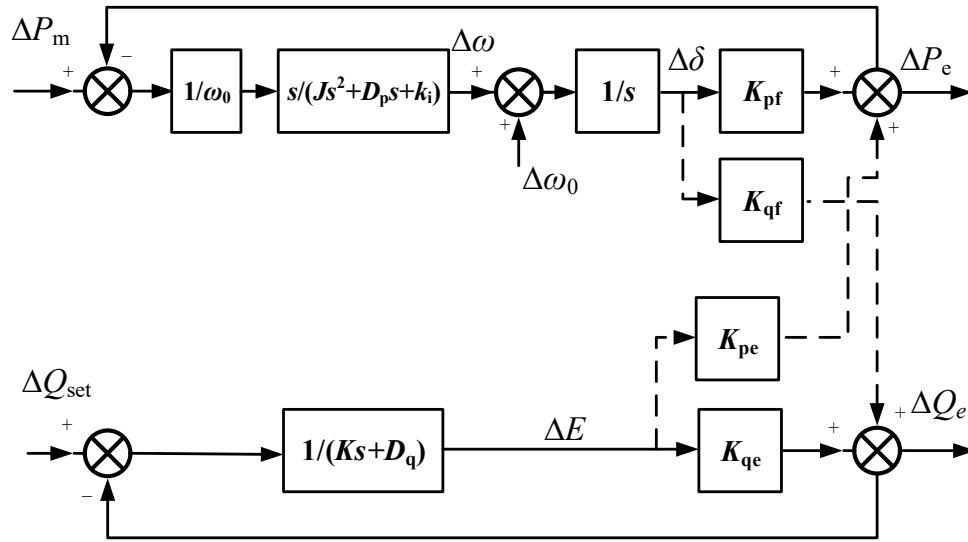


Figure 5. Small-signal equivalent model of VSG.

According to the control strategy of this paper, when the damping coefficient is too large, the closed-loop system will change from an underdamped system to an overdamped system. Therefore, the oscillation of the VSG output frequency is effectively suppressed. In the overdamped system, the settling time of the frequency response increases with the increase of the damping coefficient. To ensure that the system frequency response still has a short response time, the maximum value of  $D_p$  needs to be obtained.

When frequency disturbance occurs in the system, the primary frequency regulation of generating units should start to respond within 3 s. Therefore, the settling time  $t_s$  of the active power-frequency loop needs to be set. The time constants  $T_1$  and  $T_2$  of the overdamped second-order system are defined as follows:

$$\begin{cases} T_1 = \frac{1}{\omega_n(\zeta - \sqrt{\zeta^2 - 1})} \\ T_2 = \frac{1}{\omega_n(\zeta + \sqrt{\zeta^2 - 1})} \end{cases} \quad (11)$$

If  $T_1 \geq 4T_2$ , the system can be equivalent to a first-order system with a  $-1/T_1$  closed-loop pole [19]. Under this condition, the frequency loop settling time  $t_s = 3T_1$  is taken. The relative error is less than 10%. In this paper, the settling time is set to  $t_s < 0.5$  s. By combining Equation (11), Equation (12) can be obtained:

$$\zeta - \sqrt{\zeta^2 - 1} > \frac{6}{\omega_n} \quad (12)$$

According to Equation (12),  $\zeta < 6.213$  can be obtained. Through the relationship of  $T_1 \geq 4T_2$ ,  $1.25 < \zeta < 6.213$  can be obtained. By combining Equation (10), the maximum value of  $D_p$  is 131 Nm/s/rad.

## 5. Simulation Results

In order to verify the effectiveness and compatibility of the adaptive damping control strategy, a microgrid simulation platform is built by MATLAB/Simulink software, as shown in Figure 6. The inverters are all adopted the VSG strategy, and the capacity of the two VSGs is the same. In the island mode, two VSGs are connected in parallel to load. In the grid-connected mode, only VSG 1 is connected to the grid. The simulation parameters are shown in Table 1.

In Figure 6, the static synchronous compensator (STATCOM) can quickly output bidirectional reactive power. It consists of a DC-side capacitor and a voltage-type inverter. To ensure the stability of the output voltage amplitude, it is necessary to absorb active power from the grid to compensate for its energy loss, so it does not have active power adjustment abilities. The STATCOM with battery energy storage system (BESS) can not only quickly compensate reactive power but also provide active power support so that it can achieve more flexible power adjustment functions.

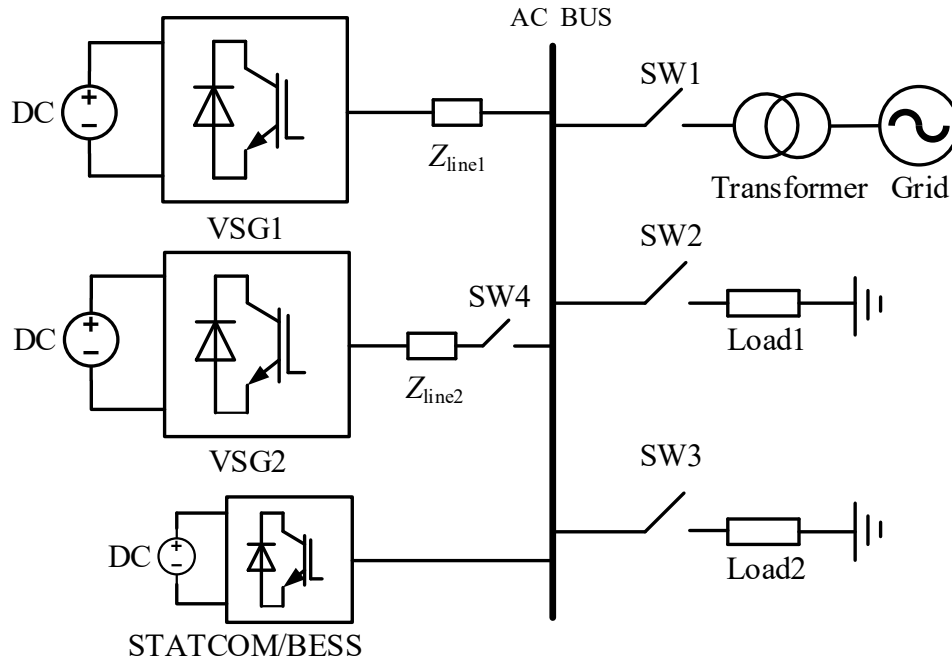


**Figure 6.** Structure diagram of simulation platform.

### 5.1. Effectiveness Test

In the island mode, through the change of the load power, the frequency stability problem caused by the system load fluctuations is simulated. Under the same simulation conditions, the control strategy of this paper is compared with the constant damping strategy (CD) and the damping strategy set based on frequency deviation (FD) [17].

For the CD strategy,  $D_p$  is set to a fixed value of 5 Nm·s/rad. For the FD strategy, the steady-state value is set to 5 Nm·s/rad. For the self-adaptive damping strategy proposed in this paper (SAD), the initial damping is set to 5 Nm·s/rad. The virtual inertia is constant, and its value  $J_0$  is set to 0.2028 kg·m<sup>2</sup>.

For a simulation of the sudden increase of load power, the active load rises from 2 kW to 10 kW at 0.6 s.

The control effects of VSG 1 under three control strategies are shown in Figure 7. For the SAD strategy, the frequency is stable in the steady-state interval ( $\pm 0.02$  Hz) at 0.665 s. For the FD strategy, the frequency is maintained in the steady-state range after 0.717 s. For the CD strategy, the frequency is maintained in the steady-state range after 0.807 s. It shows that the SAD method has a shorter settling time. The oscillation energy of frequency is quickly consumed by damping. The frequency overshoot is reduced in the second swing. The settling time and overshoot of each control strategy are shown in Table 2.

**Table 2.** Comparison of different control strategies when load increases.

Methods	CD	FD	SAD
Settling Time (s)	0.207	0.117	0.065
Overshoot (%)	0.304	0.114	0.074

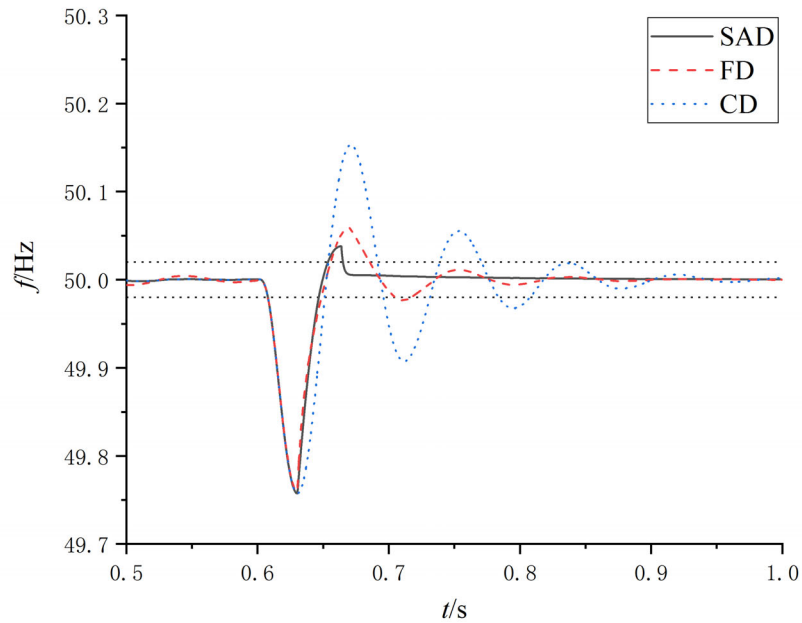


**Figure 7.** Comparison of frequency under different damping control strategies when load increases.

For a simulation of the sudden decrease of load power, the active load drops from 10 kW to 2 kW at 0.6 s. The control effects of VSG 1 are shown in Figure 8.

In Figure 8, when the load is suddenly reduced, the control effects of three strategies are the same as that of the sudden load increase. Compared with the other two strategies, the SAD strategy has less settling time and less overshoot.

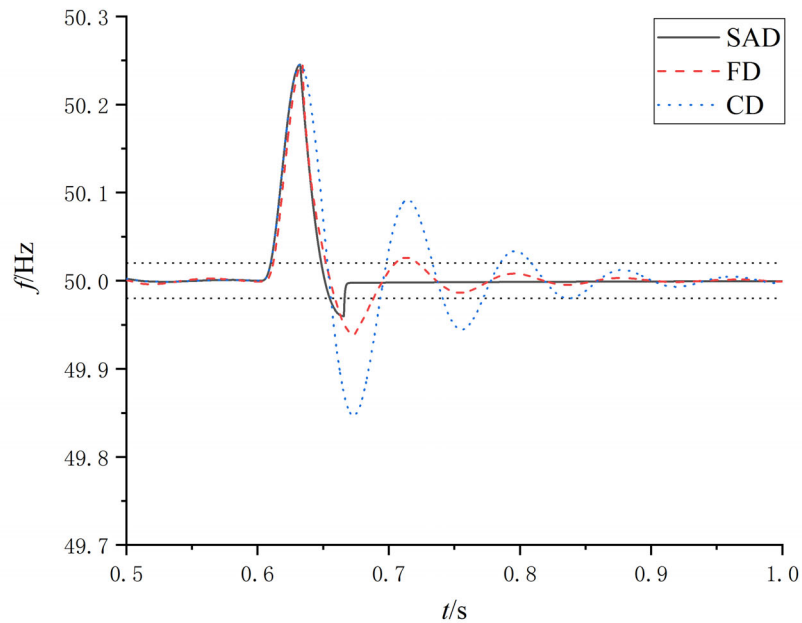


**Figure 8.** Comparison of frequency under different damping control strategies when load decreases.

In the grid-connected mode, first, VSG1 operates independently with two loads. The pre-synchronization control is turned on at 0.1 s to avoid power impact when grid-connected and island modes are switched. The active power reference of VSG 1 increased from 5 kw to 10 kw in 0.4 s. The output frequency and active power of VSG1 are shown in Figures 9 and 10.

In Figure 9, for the SAD strategy, the frequency returns to the steady-state interval faster and does not even require a second tuning. In Figure 10, the larger damping prevents the output power from overshooting and can reach the given value in time.

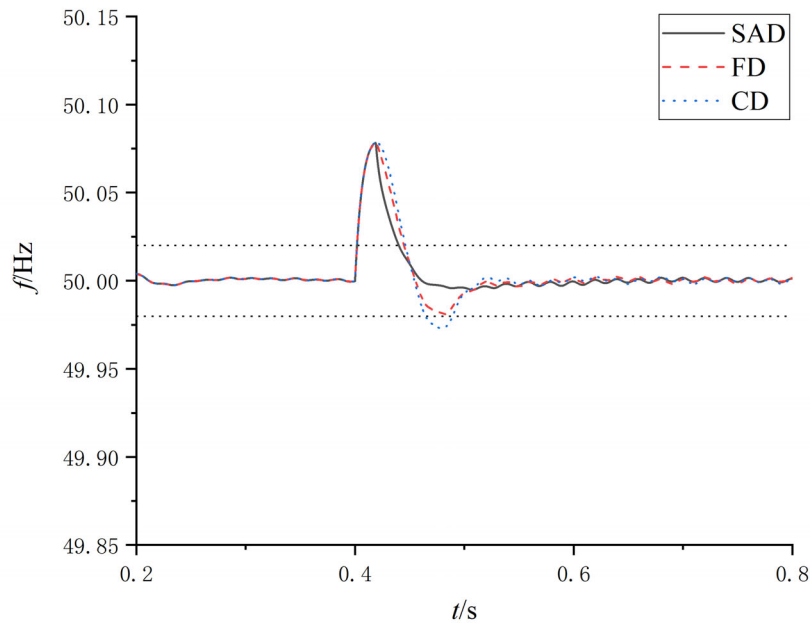


**Figure 9.** Comparison of frequency under different damping control strategies in grid-connected mode.

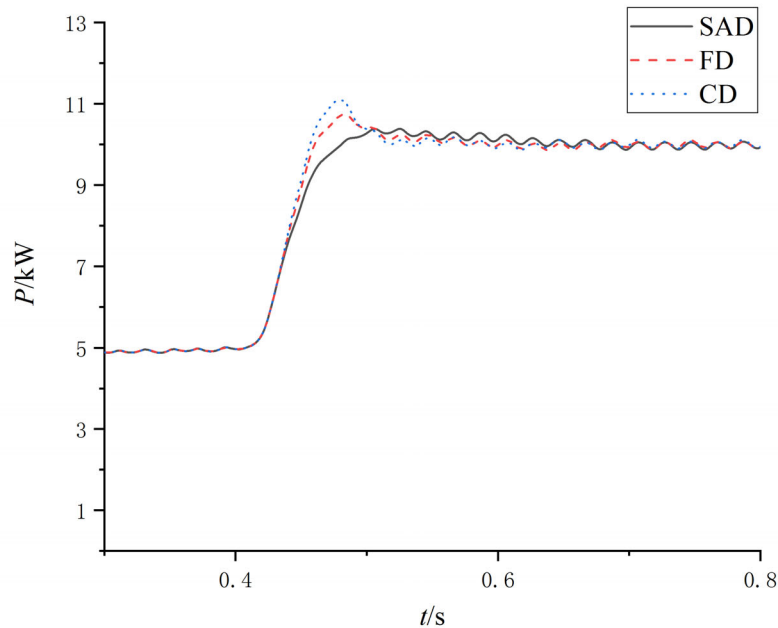


**Figure 10.** Output active power of VSG 1 under different damping control modes in grid-connected mode.

### 5.2. Compatibility Test

In order to verify the compatibility of the strategy in this paper, the damping strategy is combined with virtual inertia strategy set based on frequency change rate [17]. The three damping control strategies are the same as the above effectiveness test. The simulation system operates in the island mode. The active load rises from 2 kW to 10 kW at 0.6 s. The control effects of VSG 1 are shown in Figure 11.

In Figure 11, under the SAD strategy, the frequency response has a smaller overshoot and a shorter settling time compared with the other two strategies. The settling time and overshoot of each control strategy are shown in Table 3.

**Table 3.** Comparison of different control strategies when  $J$  is based on frequency change rate.

Methods	CD	FD	SAD
Settling Time (s)	0.151	0.098	0.054
Overshoot (%)	0.134	0.070	0.022

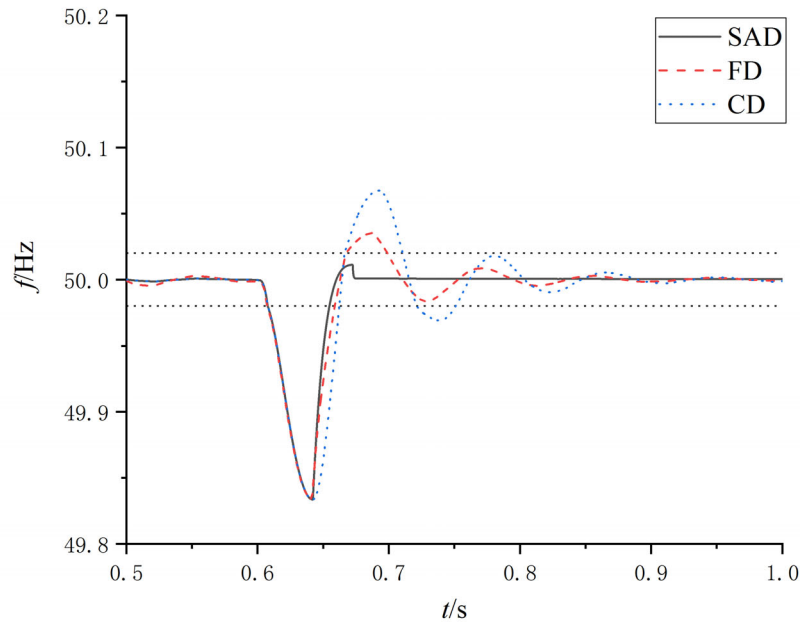


**Figure 11.** Comparison of frequency under different damping control strategies when  $J$  is based on frequency change rate.

The damping strategy is combined with virtual inertia of bang-bang control strategy [11]. The simulation conditions are the same as the previous case. The control effects are shown in Figure 12.

In Figure 12, under the SAD strategy, the frequency has no overshoot after first returning to the steady-state interval. Moreover, the frequency enters the steady-state interval faster than the other two strategies.

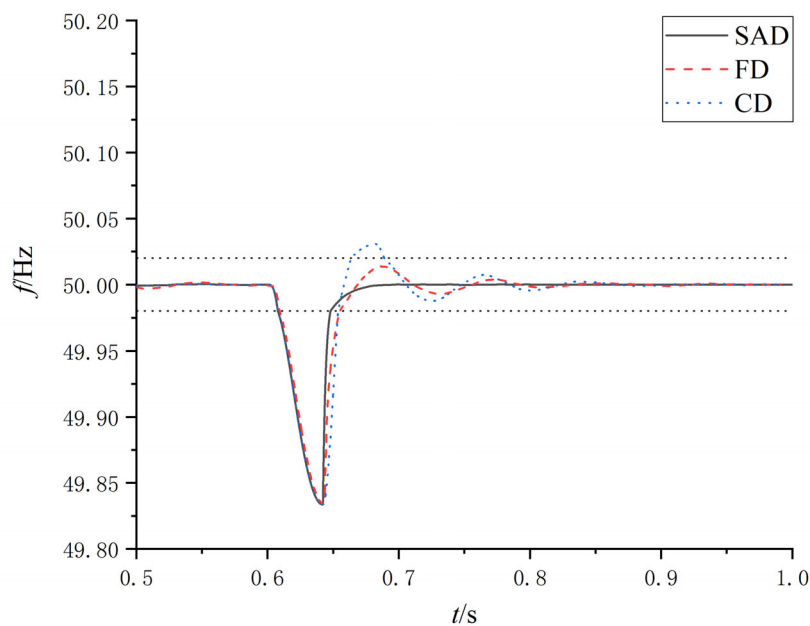


**Figure 12.** Comparison of frequency under different damping control strategies when  $J$  is based on a bang-bang control strategy.

In order to verify the applicability of the SAD strategy in the event of grid fault, the short-circuit fault in a microgrid is taken as an example. The ability of the inverter frequency recovery under different strategies is compared. The system operates in the island mode, and the initial active load is 15 kW. The three-phase short-circuit fault occurs at 0.5 s for load 1. The output frequency of VSG 1 is shown in Figure 13.

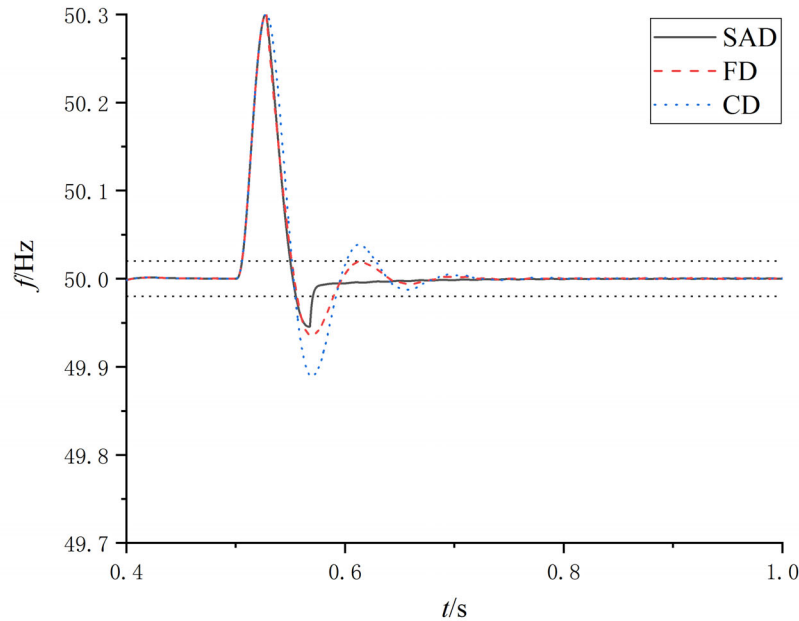


**Figure 13.** Comparison of frequency under different damping control strategies in case of a short-circuit fault.

It can be seen from Figure 13 that in case of a short-circuit fault in the grid, under the SAD method, the VSG frequency can become stable faster than the other two methods.

Under the SAD control strategy, the VSG frequency has a good dynamic response in the grid-connected or island mode. Moreover, this strategy can be combined with different virtual inertia control strategies. These simulations prove the effectiveness and compatibility of the SAD strategy.

## 6. Conclusions

In VSG, the damping term of the active power loop can slow down the frequency oscillation after the disturbance. In the underdamped system, the overshoot and the settling time of frequency response decrease with the increase of damping. Therefore, the dynamic response of frequency can be improved by increasing the damping coefficient in a certain range. According to the actual frequency maximum deviation, a self-adaptive damping (SAD) control strategy is proposed to adjust the damping value in the dynamic process. The value range of the damping coefficient is determined by establishing a small-signal model of the VSG. Through simulation experiments, the effectiveness of the SAD method is verified compared with different damping methods.

Under the SAD strategy, the response speed of VSG output power may be slowed down. In further research, the mission is to improve the dynamic response of VSG output power on the premise that the system has sufficient damping effects.

**Author Contributions:** T.L.: methodology, software, writing and editing; B.W.: review and editing; H.W.: review and editing. All authors have read and agreed to the published version of the manuscript.

**Funding:** This research was funded by the Scientific Research Project of Science and Education Park Development Center of Fuzhou University in Jinjiang City, grant number NO.2019-JJFDKY-25.

**Conflicts of Interest:** The authors declare no conflict of interest.

## References

1. Kjaer, S.B.; Pedersen, J.K.; Blaabjerg, F. A review of single-phase grid-connected inverters for photovoltaic modules. *IEEE Trans. Ind. Appl.* **2005**, *41*, 1292–1306.
2. Blaabjerg, F.; Teodorescu, R.; Liserre, M.; Timbus, A.V. Overview of Control and Grid Synchronization for Distributed Power Generation Systems. *IEEE Trans. Ind. Electron.* **2006**, *53*, 1398–1409.
3. Islam, F.M.R.; Mamun, K.A.; Oo, A.M.T. Smart Energy Grid Design for Island Countries: Challenges and Opportunities. *Green Energy Technol.* **2017**, doi:10.1007/978-3-319-50197-0.
4. Barklund, E.; Pogaku, N.; Prodanovic, M.; Hernandez-Aramburo, C.; Green, T.C. Energy Management in Autonomous Microgrid Using Stability-Constrained Droop Control of Inverters. *IEEE Trans. Power Electron.* **2008**, *23*, 2346–2352.
5. Vasquez, J.C.; Guerrero, J.M.; Luna, A.; Rodriguez, P.; Teodorescu, R. Adaptive Droop Control Applied to Voltage-Source Inverters Operating in Grid-Connected and Islanded Modes. *IEEE Trans. Ind. Electron.* **2009**, *56*, 4088–4096.
6. Mohamed, Y.A.I.; El-Saadany, E.F. Adaptive Decentralized Droop Controller to Preserve Power Sharing Stability of Paralleled Inverters in Distributed Generation Microgrids. *IEEE Trans. Power Electron.* **2008**, *23*, 2806–2816.
7. Majumder, R.; Chaudhuri, B.; Ghosh, A.; Majumder, R.; Ledwich, G.; Zare, F. Improvement of Stability and Load Sharing in an Autonomous Microgrid Using Supplementary Droop Control Loop. *IEEE Trans. Power Syst.* **2010**, *25*, 796–808.
8. Zhong, Q.; Weiss, G. Synchronverters: Inverters That Mimic Synchronous Generators. *IEEE Trans. Ind. Electron.* **2011**, *58*, 1259–1267.
9. Zhong, T.Q.; Nguyen, P.; Ma, Z.; Sheng, W. Self-Synchronized Synchronverters: Inverters Without a Dedicated Synchronization Unit. *IEEE Trans. Power Electron.* **2014**, *29*, 617–630.
10. Liu, J.; Miura, Y.; Ise, T. Comparison of Dynamic Characteristics Between Virtual Synchronous Generator and Droop Control in Inverter-Based Distributed Generators. *IEEE Trans. Power Electron.* **2016**, *31*, 3600–3611.
11. Alipoor, J.; Miura, Y.; Ise, T. Power System Stabilization Using Virtual Synchronous Generator With Alternating Moment of Inertia. *IEEE J. Emerg. Sel. Top. Power Electron.* **2015**, *3*, 451–458.
12. Shintai, T.; Miura, Y.; Ise, T. Oscillation Damping of a Distributed Generator Using a Virtual Synchronous Generator. *IEEE Trans. Power Deliv.* **2014**, *29*, 668–676.
13. Torres, M.A.L.; Lopes, L.A.C.; Morán, L.A.T.; Espinoza, J.R.C. Self-Tuning Virtual Synchronous Machine: A Control Strategy for Energy Storage Systems to Support Dynamic Frequency Control. *IEEE Trans. Energy Convers.* **2014**, *29*, 833–840.
14. Meng, X.; Liu, J.; Liu, Z. A Generalized Droop Control for Grid-Supporting Inverter Based on Comparison Between Traditional Droop Control and Virtual Synchronous Generator Control. *IEEE Trans. Power Electron.* **2019**, *34*, 5416–5438.
15. Liu, J.; Miura, Y.; Ise, T. Fixed-Parameter Damping Methods of Virtual Synchronous Generator Control Using State Feedback. *IEEE Access* **2019**, *7*, 99177–99190.
16. Dong, S.; Chen, Y.C. Adjusting Synchronverter Dynamic Response Speed via Damping Correction Loop. *IEEE Trans. Energy Convers.* **2017**, *32*, 608–619.
17. Li, D.; Zhu, Q.; Lin, S.; Bian, X.Y. A Self-Adaptive Inertia and Damping Combination Control of VSG to Support Frequency Stability. *IEEE Trans. Energy Convers.* **2017**, *32*, 397–398.

18. Zheng, T.; Chen, L.; Wang, R.; Li, C.; Mei, S. Adaptive damping control strategy of virtual synchronous generator for frequency oscillation suppression. In Proceedings of the 12th IET International Conference on AC and DC Power Transmission (ACDC 2016), Beijing, China, 28–29 May 2016; pp. 1–5.
19. Hu, S. *Automation Control Theory*, 5th ed.; Science Publishing House: Beijing, China, 2007.
20. *Requirements for the Connection of Micro Generators in Parallel with Public Low-Voltage Distribution Networks*; EN 50438; CEI: Houston, TX, USA, 2008.
21. Asiminoaei, L.; Teodorescu, R.; Blaabjerg, F.; Borup, U. A digital controlled PV-inverter with grid impedance estimation for ENS detection. *IEEE Trans. Power Electron.* **2005**, *20*, 1480–1490.
22. Bevrani, H.; Shokoohi, S. An Intelligent Droop Control for Simultaneous Voltage and Frequency Regulation in Islanded Microgrids. *IEEE Trans. Smart Grid* **2013**, *4*, 1505–1513.
23. Wu, H.; Ruan, X.; Yang, D.; Chen, X.; Zhao, W.; Lv, Z.; Zhong, Q. Small-Signal Modeling and Parameters Design for Virtual Synchronous Generators. *IEEE Trans. Ind. Electron.* **2016**, *63*, 4292–4303.



© 2020 by the authors. Licensee MDPI, Basel, Switzerland. This article is an open access article distributed under the terms and conditions of the Creative Commons Attribution (CC BY) license (<http://creativecommons.org/licenses/by/4.0/>).